PASJ: Publ. Astron. Soc. Japan **48**, 395–407 (1996)

Metal Abundance of an X-Ray Emitting Gas in Two Groups of Galaxies: The NGC 5044 Group and HCG 51

Yasushi FUKAZAWA,[1] Kazuo MAKISHIMA,[1] Kyoko MATSUSHITA,[1]
Noriko YAMASAKI,[2] Takaya OHASHI,[2] Richard F. MUSHOTZKY,[3]
Yasuhiro SAKIMA,[4] Yoshiyuki TSUSAKA,[4,5] and Koujun YAMASHITA[4]

[1]*Department of Physics, School of Science, University of Tokyo, 7-3-1 Hongo, Bunkyo-ku, Tokyo 113*
E-mail(YF): fukazawa@miranda.phys.s.u-tokyo.ac.jp
[2]*Department of Physics, Faculty of Science, Tokyo Metroplitan University, Hachioji, Tokyo, 192-03*
[3]*Code 666, NASA/ Goddard Space Flight Center, Greenbelt, MD 20771, U.S.A.*
[4]*Department of Physics, Faculty of Science, Nagoya University, furocho, chikusa-ku, Nagoya 464-01*
[5]*Institute for Molecular Science, Okazaki, Aichi 444*

(Received 1995 November 21; accepted 1996 April 16)

Abstract

We observed two groups of galaxies, the NGC 5044 group (WP 23) and Hickson's compact group HCG 51, with ASCA. We detected an extended bright soft X-ray emission, which indicates the existence of large amounts of a hot X-ray emitting gas in both targets. The temperature of the hot gas is ~ 1 keV for both objects, which is equivalent to their galaxy velocity dispersion. The metal abundance of the gas is 0.3–0.5 solar value for both objects, which is similar to that of rich clusters of galaxies. The Si to Fe abundance ratio is smaller than that of rich clusters of galaxies, although the iron abundances determined by the Fe-L lines are somewhat uncertain. The X-ray luminosities in the 0.5–10 keV band are 1×10^{43} erg s^{-1} and 5×10^{42}erg s^{-1} for the NGC 5044 group and HCG 51, respectively, which are higher by an order of magnitude than those of X-ray bright elliptical galaxies. This makes HCG 51 one of the most X-ray luminous compact groups. Both objects have a total gravitating mass of $M_{\rm total} \sim 2.0 \times 10^{13}\,M_\odot$, and a gas mass and a galaxy mass of $M_{\rm gas} \sim M_{\rm galaxy} \sim 1.5 \times 10^{12}\,M_\odot$. The ratios among these mass components are $M_{\rm gas}/M_{\rm galaxy} \sim 1$ and $(M_{\rm gas}+M_{\rm galaxy})/M_{\rm total} \sim 0.2$ within $\sim$350 kpc for both objects. The latter is similar to previous ROSAT results for many groups of galaxies, while the former is larger than the average value of the ROSAT-observed groups. Moreover, the metal abundances of the present two groups are significantly higher than those of the NGC 2300 group and HCG 62, and are comparable to those of clusters. These suggest that the hot-gas mass and metal abundances can scatter widely among groups, compared to the small variance found among rich clusters.

Key words: Galaxies: abundances — Galaxies: clusters of — Galaxies: individual (NGC 5044, HCG 51) — Galaxies: intergalactic medium

1. Introduction

It is generally known that the mass of clusters of galaxies and elliptical galaxies consists of three distinct components: visible galaxies (or stars), X-ray emitting hot gas, and dark matter. The ratios among these three components are important for characterizing the two classes of systems. Since the latter two components can be most efficiently studied through X-ray imaging spectroscopy, extensive investigations have been carried out using the Einstein observatory (e.g., Jones, Forman 1984; Forman et al. 1985), EXOSAT (e.g., Edge, Stewart 1991), and ROSAT (e.g., David et al. 1995). According to these previous studies, although the mass ratio between luminous matter ($M_{\rm lum} = M_{\rm gas} + M_{\rm galaxy}$, where $M_{\rm gas}$ is the gas mass and $M_{\rm galaxy}$ is the galaxy mass) and the total matter $M_{\rm total}$ is about 0.1–0.2 (for an assumed Hubble constant of H_0= 50 km s^{-1} Mpc^{-1}) for both classes of systems, the ratio $M_{\rm gas}/M_{\rm galaxy}$ is considerably different between them. Clusters have $M_{\rm gas}/M_{\rm galaxy} = 2$–5, while elliptical galaxies have $M_{\rm gas}/M_{\rm galaxy} < 0.1$.

The hot gas in these systems contains some fraction of metal-rich gas, which is processed in the stellar interior and then ejected into interstellar/intergalactic space. Observations from HEAO-1 (Rothenflug, Arnaud 1985), EXOSAT (Edge, Stewart 1991), Ginga (Awaki et al. 1991; Hatsukade 1989; Tsuru 1992), and ASCA (Awaki et al. 1994; Matsushita et al. 1994) have shown that the

metal abundances of the hot gas are similar at about 0.3–0.6 solar for both systems, in spite of the large difference in their $M_{\rm gas}/M_{\rm galaxy}$ ratios. Since the mass of the processed hot gas relative to $M_{\rm galaxy}$ is considerably smaller in elliptical galaxies than in clusters, it is likely that most of the processed hot gas ejected from stars has escaped into intergalactic space rather than being confined in the vicinity of the elliptical galaxies. These results suggest that clusters of galaxies are closed systems to both the primordial and metal-rich gas, while elliptical galaxies are systems open to both of these gaseous components (Tsuru 1992).

Then, how about groups of galaxies, which form an intermediate class of systems between clusters and individual galaxies? X-ray observations of groups of galaxies have recently started, and the existence of extended X-ray emitting hot gas has been confirmed in many groups by ROSAT (Ebeling et al. 1994; Pildis et al. 1995). ROSAT observations have indicated that the $M_{\rm lum}/M_{\rm total}$ ratio has a median value of ~ 0.2 (Mulchaey et al. 1996). This value is roughly the same as those of clusters of galaxies and elliptical galaxies, and may be fairly common for all of these bound systems. However, the $M_{\rm gas}/M_{\rm galaxy}$ ratio seems to scatter widely amongst groups (Pildis et al. 1995; Mulchaey et al. 1996), suggesting that groups are located at the threshold between open and closed systems. Moreover the ROSAT data suggest metal abundances as low as 0.1–0.2 solar in some groups (Mulchaey et al. 1993; Ponman, Bertram 1993), which has been confirmed by ASCA for the NGC 2300 group and HCG 62 (Sakima et al. 1994). This is significantly lower than those of clusters of galaxies, suggesting that these groups may have lost a considerable amount of metal-rich gas. However, the sample is still too small to conclude whether this is a common characteristic of the groups or not.

ASCA (Tanaka et al. 1994) has a very good energy resolution, a wide energy band, and a moderate angular resolution, which are all essential for determining the temperature and metal abundances of extended hot gas. In particular, ASCA can resolve various atomic emission lines expected in the X-ray spectra of groups. In this paper, we report ASCA observations of two groups of galaxies, the NGC 5044 group and the Hickson's compact group No.51 (HCG 51). A comparison of these objects with other groups is also presented. We assume $H_0 = 50$ km s^{-1} Mpc^{-1} in this paper.

2. Observation and Data Reduction

Galaxy groups may form a relatively inhomogeneous class of systems, with a considerable scatter in their optical parameters, which include the total number, velocity dispersion, density, and morphology of the member galaxies. For example, among the well-studied X-ray emitting groups, HCG 62 has two dominant galaxies, and only two other dwarf galaxies, while the NGC 2300 group is a very loose system containing only four galaxies. Nevertheless, the velocity dispersion is ~ 300 km s^{-1} for both. In order to clarify how the hot-gas properties of galaxy groups depend on these group characteristics, we must also study groups with a larger number of galaxies, higher galaxy density, and larger velocity dispersion than these two examples. We have selected the NGC 5044 group and HCG 51 for our study.

Table 1. Optical parameters of the two groups.

	NGC 5044 group*	HCG 51†
Galaxy density (Mpc^{-3})	12×10^2	5×10^2
Redshift	0.0087	0.0262
Velocity dispersion (km s^{-1})	474	467
Number of galaxies	$\sim$100	$\sim$7
M/L $(M/L)_\odot$	$\sim$300	$\sim$72

* Ferguson et al. (1990)
† Hickson et al. (1988); Hickson (1993)

The NGC 5044 group (WP 23) is a nearby well-studied group of galaxies. A giant elliptical galaxy, NGC 5044, is located at the center, and many dwarf galaxies exist around it. In table 1 its optical parameters are listed. Its mean redshift is $z = 0.0087$, and it has a more concentrated galaxy distribution than does the Fornax cluster, another well-studied poor cluster. The Einstein Observatory detected extended emission around NGC 5044 (Fabbiano et al. 1992), while Ginga detected a soft thermal component and a power-law hard component with a photon index of 1.7 (Y. Ikebe, private communication), which prevented an investigation of the temperature and metal abundance of the hot gas. David et al. (1994) accurately measured the X-ray surface-brightness distribution with ROSAT, and obtained $M_{\rm gas}/M_{\rm galaxy} \sim 1$ and $M_{\rm lum}/M_{\rm total} \sim 0.2$ within 350 kpc. The X-ray surface brightness exhibits a sharp increase towards the center, and the spectrum in the central region indicates the presence of a cool component, which they interpret to be a cooling flow. An ASCA observation of the NGC 5044 group was briefly reported in Mushotzky (1994) and Tsusaka et al. (1994).

In order to compare the NGC 5044 group with more compact systems without a central dominant galaxy, we selected a target from the sample of Hickson Compact Galaxy Catalogue (Hickson et al. 1988). We applied the following criteria: the object should have a moderate number of galaxies, a high galaxy density, a large velocity dispersion, and no AGN (active galactic nuclei) candidates, and that it is not too distant. Only HCG 51 satisfied these conditions. It contains 7 galaxies, five of

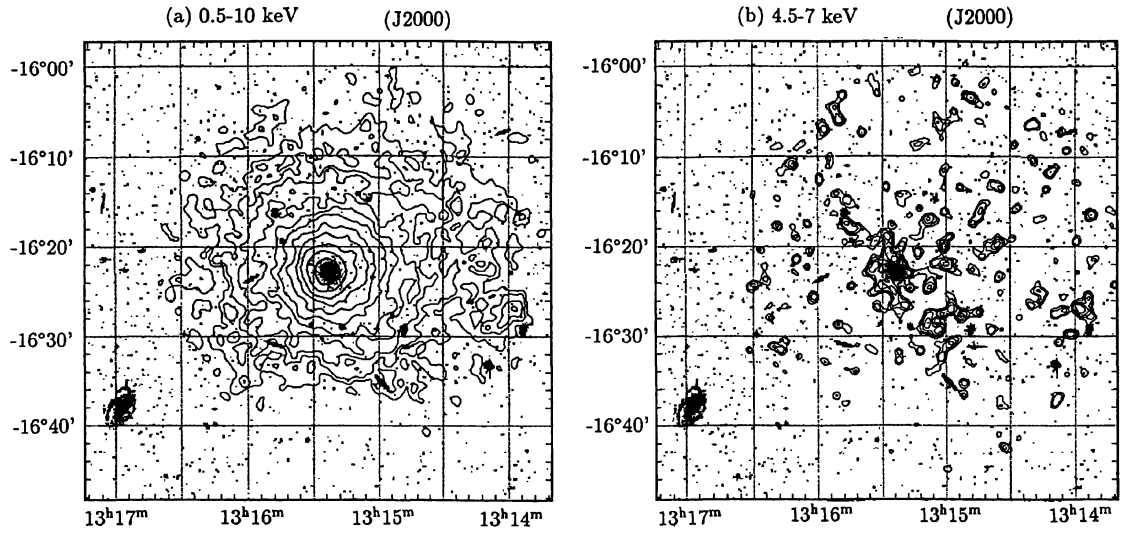

Fig. 1. GIS2+3 images of the NGC 5044 group presented in the J2000 coordinates, superposed on the optical image (gray scale). (a) In the 0.5–10 keV band. (b) In the 4.5–7 keV band. Both images have been smoothed with a Gaussian filter of $\sigma = 0'.5$. The contour levels are logarithmically spaced by a factor of 1.46 and 1.27 for (a) and (b), respectively. The background is not subtracted.

which have similar optical luminosities within a factor of ~ 3. The velocity dispersion, 470 km s^{-1} or equivalent to ≥ 1 keV, is thought to be high enough to bind a significant amount of hot gas. Although HCG 51 was detected in the ROSAT All Sky Survey (Ebeling et al. 1994), its detailed hot gas properties have not been well studied.

We observed the NGC 5044 group with ASCA on 1993 June 20–21, during the PV (performance verification) phase. As a result of an error in the satellite operation, the attitude changed by 10′ during the observation, and, consequently, two pointings were performed. The effective observation time is 8.9 ks for one pointing, and 19.3 ks for the other. The observation mode was the normal PH mode for the GIS (Ohashi et al. 1991; Kohmura et al. 1993; Ohashi et al. 1996) and the 4CCD Faint/Bright mode for the SIS (Burke et al. 1991). HCG 51 was observed on 1994 June 3–4, in the AO-2 phase, for an effective time of 75 ks. The observation mode was the PH normal mode for the GIS and the 2CCD/1CCD Faint mode for the SIS.

For both objects, we accumulated the detected events under the condition of a telescope viewing direction of $> 5°$ from the dark Earth rim, and a magnetic cutoff rigidity > 10 GeV c^{-1}. This was to minimize any fluctuation of the particle background, which is particularly important in studying extended emission with a low surface brightness. Moreover, we imposed the condition of a telescope viewing direction of $> 25°$ from the bright Earth rim for the SIS data, in order to avoid the effect of light leakage on the CCD chips.

3. Image Analysis

In figure 1 we show the GIS images of the NGC 5044 group in the total band (0.5–10 keV) and the hard band (4.5–7 keV). The GIS count rate in the 0.5–10 keV band was 0.7 c s^{-1} sensor^{-1}. Extended emission over the full GIS field of view (of diameter 50′) can be seen around NGC 5044, with an approximate circular symmetry. In the hard-band image, the extended emission is very weak, and several individual sources can be seen, including NGC 5044, itself. The 2–10 keV X-ray fluxes of these sources are about 3×10^{-13} erg s^{-1} cm^{-2}, and their luminosities are 1×10^{41} erg s^{-1} if they are at the redshift of the group. They are too faint to account for a bright hard spectral component detected by Ginga from the NGC 5044 field, with a 2–10 keV flux of $\sim 7\times10^{-12}$ erg s^{-1} cm^{-2}. Probably, the hard component detected with Ginga came from a point source located at $> 30'$ away from NGC 5044, although we cannot rule out the possibility that one of the hard sources detected with ASCA varied by an order of magnitude.

In figure 2 the GIS and SIS images of HCG 51 are shown. We can see strong X-ray emission at the position of HCG 51 with GIS count rate of 0.05 c s^{-1} sensor^{-1}. The peak of the X-ray intensity is coincident within 0′.5

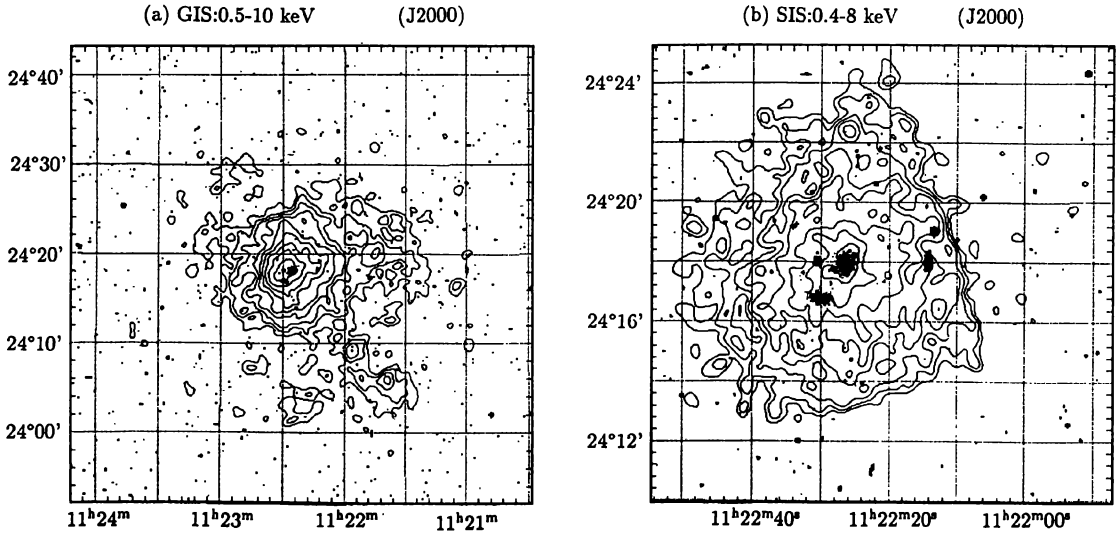

Fig. 2. X-ray images of HCG 51 superposed on the optical image. (a) The GIS2+3 image in the 0.5–10 keV band. (b) The SIS0+1 image in the 0.4–7 keV band. The images have been smoothed with a Gaussian filter of $\sigma = 0'.5$ and $\sigma = 0'.3$, for (a) and (b), respectively. The contour levels are logarithmically spaced by a factor of 1.26 for both figures. The background is not subtracted. The gray scale represents the optical image.

with the elliptical galaxy NGC 3651, the brightest member in HCG 51. The emission is significantly extended up to 7′, implying that HCG 51 also contains a significant amount of hot gas. There is an asymmetric emission to the west in the outer region. Although not shown separately, the X-ray emission in the hard band is very weak, confirming that none of the members of HCG 51 are significant AGN candidates.

We extracted azimuthally averaged radial profiles of the GIS image in the 1–2 keV band from both objects, to fit them with a β-model (Cavaliere, Fusco-Femiano 1976). This model represents the surface brightness as $S_0[1 + (r/r_c)^2]^{-3\beta+\frac{1}{2}}$, where r is the projected distance from the emission centroid, while S_0, r_c, and β are model parameters to be adjusted. For HCG 51, the asymmetric region to the west, whose position angle is from 193° to 343°, was excluded. The background was subtracted in a way as described later. The β-model was multiplied by the XRT vignetting function, and was then convolved with the 1–2 keV point-spread function of the XRT+GIS, for which we employed the actually observed GIS image of CygX-1.

The radial profiles of both systems are fitted rather well with the β-model, with a χ^2/d.o.f. of 118/97 for the NGC 5044 group and 56/47 for HCG 51. In figure 3 the radial profiles and best-fit β-models are shown. The obtained model parameters are $\beta = 0.53 \pm 0.03$ and $r_c = 1'.00 \pm 0'.25$ for the NGC 5044 group, and $\beta = 0.60 \pm 0.05$ and $r_c = 1'.7 \pm 0'.5$ for HCG 51. Here, the errors represent single-parameter 90% confidence limits. The derived core radii are rather small, 15 kpc for the NGC 5044 group and 77 kpc for HCG 51. For the NGC 5044 group, David et al. (1994) derived $\beta = 0.53 \pm 0.02$ and $r_c = 1'.8 \pm 0'.7$ with ROSAT. The ASCA result concerning β is quite consistent with the ROSAT result, though r_c seems smaller than the ROSAT value. This may be because David et al. (1994) excluded the central region ($r < 3'.5$), where the ROSAT image exhibits a sharp excess; since ASCA cannot resolve this central excess, we fitted the radial profile including the central region. HCG 51 is inferred to have a flatter surface brightness at the center than does the NGC 5044 group. In the central region, the gas density is estimated to be 2.1×10^{-2} cm^{-3} and 2.0×10^{-3} cm^{-3} for the NGC 5044 group and HCG 51 respectively, although the former may be underestimated because of the relatively coarse angular resolution of ASCA.

4. Spectral Analysis

For the spectral analysis, we added all available data from different sensors, chips, modes, and pointings for the GIS and the SIS separately after an appropriate gain correction. The background spectra were made from several blank-sky data, such as NEP (North Ecliptic Pole), Draco, and QSF 3 fields; we then subtracted them from the on-source spectra. The precise energy-response ma-

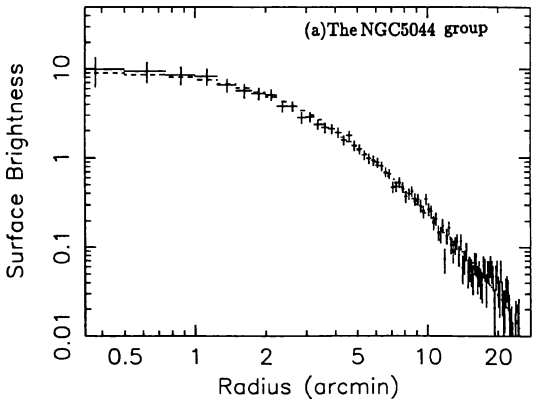

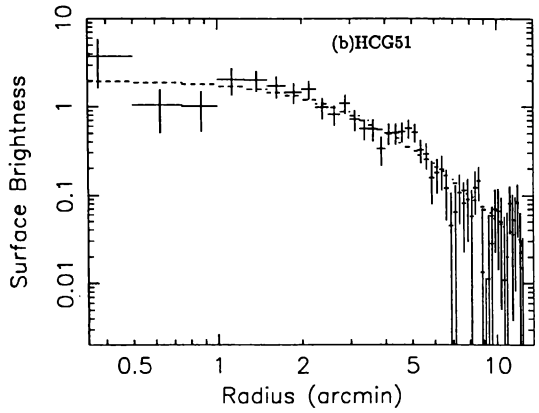

Fig. 3. Background-subtracted radial X-ray brightness profiles of (a) the NGC 5044 group and (b) HCG 51, obtained with the GIS in the 1–2 keV band. The instrumental response is not removed. The dashed lines represent the best-fit β-model convolved with the XRT+GIS PSF.

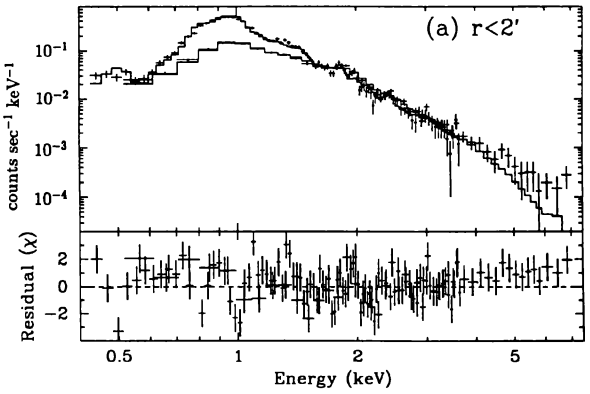

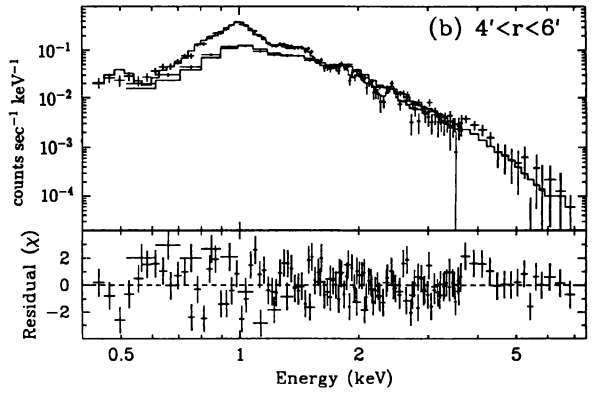

Fig. 4. GIS and SIS spectra of the NGC 5044 group, jointly fitted with a single-temperature Raymond-Smith plasma model in which abundances of five element groups are left free to vary (see text). The crosses represent the observed data, while the lines represent the best-fit model convolved through respective instrument responses. (a) For $r < 2'$. (b) For $4' < r < 6'$.

trices of the ASCA instruments for extended sources are not yet currently available, due to the complex characteristics of the X-ray telescope. However, both groups have relatively soft X-ray spectra, and the effect of uncertainty in the response matrices is thought to be small, because the temperature is almost determined by the shape of the Fe-L line complex. Accordingly, we used the energy response matrices for point sources.

Since the treatment of the Fe-L lines is known to differ significantly among the plasma emission models, the fitting results depend considerably on the choice of model (e.g., Fabian et al. 1994; Arimoto 1996). We used several plasma-emission models, including the Raymond-Smith (R-S model: Raymond, Smith 1977), Mewe-Kaastra (Meka model: Mewe et al. 1985; Mewe et al. 1986), Masai84 (Masai 1984), and Masai94 (K. Masai, private communication) models, to estimate systematic differences in the derived plasma properties. The Masai84 model uses the ionization and recombination rate coefficients compiled by Kato, Masai (1984) for all of the elements, while the Masai94 model uses those revised by Arnaud, Raymond (1992) for Fe and those compiled by Arnaud, Rothenflug (1985) for the other elements.

Table 2. The reduced χ^2 of the single-temperature fits to the spectra of the NGC 5044 group using various plasma models.*

Radius range	$< 2'$	$2'$–$4'$	$4'$–$6'$	$6'$–$8'$	$8'$–$10'$	$10'$–$15'$
R-S	1.79	2.46	1.49	1.30	1.26	1.11
Meka	4.02	4.47	3.12	2.07	1.48	1.53
Masai84	1.53	2.13	1.42	1.28	1.13	1.13
Masai94	1.78	2.70	1.61	1.20	1.25	1.20

* The GIS and the SIS spectra are fitted jointly. The degree of freedom is ~ 130 for inner regions and ~ 100 for outer regions. See text for the model description.

4.1. *The NGC 5044 group*

Since the NGC 5044 group has a well-resolved image with high photon statistics, we made six spectra for ring-shaped regions of various projected radii r from the group center, with boundaries at $2'$, $4'$, $6'$, $8'$, $10'$, and $15'$. Figure 4 shows two representative spectra, for $r < 2'$ and for $4' < r < 6'$, in which many strong lines can be seen. The shape of the Fe-L line complex apparently depends on the radius, indicating radial changes in the spectrum. We fitted these GIS and SIS spectra jointly with each of the four single-temperature plasma-emission models described above. The free parameters of the fits were the column density, temperature, normalization, and abundances of O, Mg, Si, S, and Fe. This is because the lines of these elements, except for Mg, are significant in the spectra, and their abundances are thought to be well constrained. The abundances of Ne and Al are tied to be the same as that of O; Ca and Ar to be the same as S; and Ni to be the same as Fe. The abundances of C and N are fixed at the solar value. The abundance ratios are taken from the solar photospheric values in Anders and Grevesse (1989), with $(\mathrm{Fe/H})_\odot = 4.8\times10^{-5}$. In our analysis, the abundance of Mg becomes quite small, probably due to a plasma-code problem involving confusion with some Fe-L lines (Fabian et al. 1994); we thus ignored the derived Mg abundance.

The reduced χ^2 values from those fits are sometimes large, as shown in table 2. The fits are not improved, however, by adding another temperature component. The residuals are large around the Fe-L line complex, which is thought to be due to uncertainties in the plasma emission model and the response matrix. On the other hand, these spectra do not show a hard tail, which is generally seen in the spectra of elliptical galaxies, and is attributed to the integrated emission from discrete sources (Matsushita et al. 1994). The derived upper limit on the 2–10 keV luminosity of the hard component for $r < 5'$ is 1.2×10^{41} erg s^{-1}, which gives an upper limit on L_{hard}/L_B, 3-times larger than that seen in typical elliptical galaxies.

We derived radial profiles of the temperature, metal abundances, and column density for various plasma models by analyzing the six ring-sorted spectra in the same way. The results are shown in figure 5; the results for the central $r < 2'$ region and the outer $4' < r < 6'$ region are also tabulated in table 3. The temperature is thus strongly dependent on the plasma models (figure 5a). This effect is mainly caused by differences among the plasma models in their treatment of the Ne-like Fe^{+16} ion, which has a stable electronic shell structure, and gives a significant contribution to the Fe-L lines, and the fraction, of which is different among models, even for the same temperature. In the spectral fitting, the shape of the Fe-L line complex primarily determines the temperature, and, hence, the obtained temperature depends on the plasma models. The Meka model gives a significantly lower temperature than does the R-S model, in agreement with a report by Fabian et al. (1994). The metal abundances and column density are also dependent on the models. However, the tendency of the temperature decreasing toward the center is common among the models; hence, this effect seems to be real. In the outer regions the R-S temperature is about 1 keV, and decreases to 0.8 keV toward the central region, in agreement with the ROSAT results (David et al. 1994, who used the R-S model).

To check which of the plasma models gives the most reasonable temperatures, we fitted the data in energies above 1.5 keV, where there are no strong Fe-L lines, with a model consisting of bremsstrahlung and four gaussian lines. These lines represent hydrogenic and helium lines from Si and S. We find that the fitted bremsstrahlung temperature is consistent with those derived in the R-S, Masai84, and Masai94 models.

The obtained abundance profiles of O, Si, and S (figures 5c, d, e) are relatively uniform, with at most weak negative gradients. For the Fe abundance, the R-S model indicates a relatively uniform distribution, while a negative gradient of factor 2–3 is indicated by other models, especially by the Masai94 model (figure 5f). Although there remain some uncertainties in the absolute value of iron abundance determined by Fe-L lines, the model-dependent uncertainty in the metallicity seems to be small in the outer region. These results indicate that metal abundances of the NGC 5044 group are 0.3–0.5 solar, except in the central region ($r < 5'$), where there is a hint of an increased Fe abundance. We note that the Si and S abundances are about the same as that of Fe, even in the outer regions. This is different from that observed in several clusters of galaxies (Mushotzky 1994; Mushotzky et al. 1996). Figure 5b shows that the column density increases toward the center for all of the models, although its absolute value is somewhat model dependent. In any case, the column density in the cen-

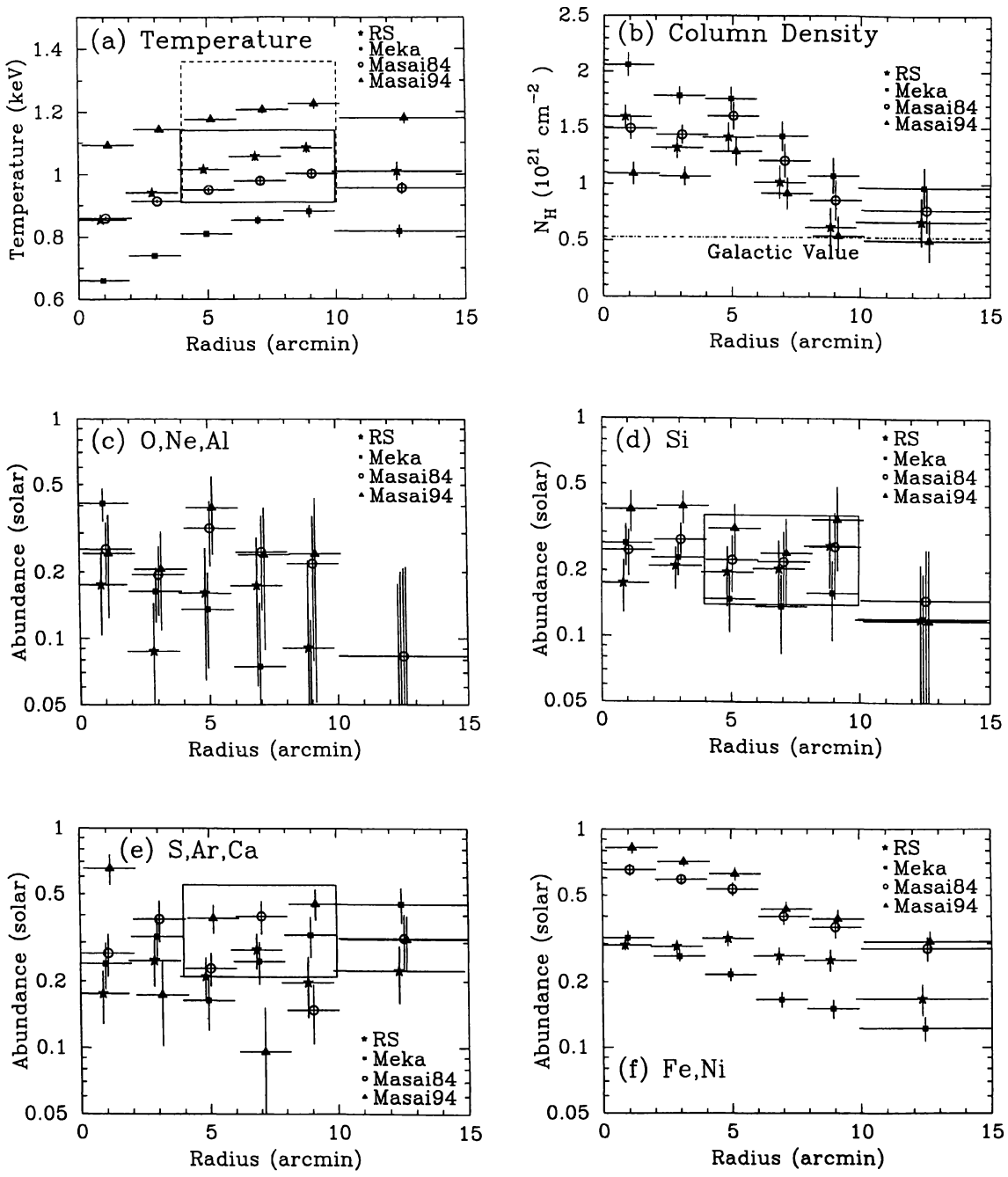

Fig. 5. Radial profiles of X-ray emission properties of the NGC 5044 group obtained by jointly fitting the GIS and SIS spectra with various plasma models. The models are explained in the text. The error bars represent the 68% confidence level. (a) Temperature. The solid and dashed boxes represent the 90% confidence regions (covering the four plasma models) of the ionization temperatures for the Si-K and S-K lines respectively, determined with the SIS. (b) Column density. (c) O, Ne, and Al abundance. (d) Si abundance. The solid box represents the 90% confidence regions (covering the four plasma models) of the Si abundance, determined by a narrow spectral region including the Si-K lines with the SIS. (e) S, Ar, and Ca abundance. The solid box represents the 90% confidence regions (covering the four plasma models) of the S abundance, determined by a narrow spectral region including the S-K lines with the SIS. (f) Fe abundance.

Table 3. Spectral parameters of the NGC 5044 group obtained by jointly fitting the GIS and SIS spectra.*

Plasma model	kT (keV)	$N_{\rm H}$ (10^{21}cm^{-2})	O (solar)	Si (solar)	S (solar)	Fe (solar)	χ^2/dof
$0' < R < 2'$							
R-S	0.85±0.01	1.6±0.1	0.17±0.07	0.17±0.05	0.24±0.06	0.29±0.02	1.79
Meka	0.66±0.01	2.1±0.1	0.41±0.07	0.27±0.06	0.65±0.10	0.32±0.02	4.02
Masai84	0.86±0.01	1.5±0.1	0.25±0.08	0.25±0.06	0.32±0.07	0.65±0.04	1.53
Masai94	1.09±0.01	1.1±0.1	0.24±0.12	0.38±0.08	0.17±0.07	0.83±0.05	1.78
$4' < R < 6'$							
R-S	1.02±0.01	1.4±0.1	0.16±0.09	0.20±0.06	0.32±0.07	0.32±0.02	1.49
Meka	0.81±0.01	1.7±0.1	0.14±0.06	0.15±0.04	0.45±0.07	0.22±0.01	3.12
Masai84	0.95±0.01	1.6±0.1	0.31±0.10	0.22±0.06	0.45±0.07	0.53±0.03	1.42
Masai94	1.18±0.01	1.3±0.1	0.39±0.15	0.31±0.09	0.31±0.08	0.62±0.04	1.61

* Errors represent 68% confidence level. Abundances of C and N are fixed to one solar.

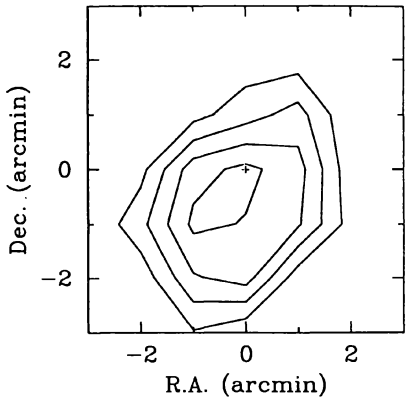

Fig. 6. Temperature map in the central region of the NGC 5044 group in terms of the R-S model, obtained with the SIS. The contour levels are 0.85, 0.90, 0.95, and 1.00 keV from inside to outside. The cross indicates the peak position of the X-ray surface brightness.

tral region exceeds the galactic value of 5.4×10^{20} cm^{-2} (Stark et al. 1992), as has been seen in cooling flow clusters (White et al. 1991). This excess absorption is required, even in the bremsstahlung + lines model, and, thus, represents the absorption of the continuum, rather than the unseen, low-energy emission lines. In terms of the R-S fit, although the iron abundance is spatially rather uniform, like the ROSAT results, the our average value of 0.20–0.30 solar is different from the ROSAT value of 0.8 solar (David et al. 1994). Although the solar ratio of (Fe/H) they used does not appear in their paper, their iron mass, $M_{\rm Fe} = 8.6 \times 10^8\,M_\odot$, in gas, and their gas mass, $M_{\rm gas} = 9 \times 10^{11}\,M_\odot$ (both within 250 kpc), taken from their figure 5, suggest that they assume $({\rm Fe/H})_\odot = 2.1 \times 10^{-5}$. If so, the ROSAT abundance is equivalent to 0.35 solar in our definition, and becomes consistent with the ASCA results.

The SIS data for the NGC 5044 group are statistically good enough to resolve spatial changes in the spectra on $2'$ angular scales, particularly changes in the shape of the Fe-L line complex, which is very sensitive to the temperature. We therefore obtained the SIS spectrum in each $2' \times 2'$ grid in the central $6' \times 6'$ region, and fitted them with the R-S model. Figure 6 is the obtained temperature map. Although absolute value of the temperature is model-dependent, as described before, the temperature gradient is thought to be real. It can be seen that the central cool region is asymmetric, in agreement with the tendency seen in the ROSAT hardness ratio map. However, the asymmetry is not too severe to make the azimuthal integration meaningless.

4.2. HCG 51

The data of HCG 51 are statistically much poorer than those for the NGC 5044 group, and the spectra for $r < 2'.5$ and $2'.5 < r < 5'$ are very similar. Therefore, we dealt with the single spectrum covering $r < 5'$. The HCG 51 spectrum thus obtained, shown in figure 7, is similar to that of the NGC 5044 group. We list the results from single-temperature spectral fits using various plasma models in table 4. Thus, some plasma models give nearly acceptable fits, while others do not. The allowed range of temperature is 1.0–1.2 keV, which is narrower than that of the NGC 5044 group. This temperature

Table 4. Spectral parameters of HCG 51 obtained by jointly fitting the GIS and SIS spectra.*

Plasma model	kT (keV)	N_H (10^{21} cm^{-2})	O (solar)	Si (solar)	S (solar)	Fe (solar)	χ^2/dof
R-S	1.10±0.01	1.6±0.2	<1.00	0.20±0.07	0.24±0.08	0.25±0.02	1.37
Meka	0.95±0.02	1.8±0.2	<1.00	0.12±0.05	0.24±0.07	0.16±0.02	1.91
Masai84	1.04±0.02	1.8±0.2	<1.00	0.18±0.07	0.26±0.08	0.33±0.03	1.40
Masai94	1.27±0.02	1.5±0.2	<1.00	0.29±0.10	0.17±0.10	0.35±0.03	1.20

* Errors represent 68% confidence level. Abundances of C and N are fixed to one solar.

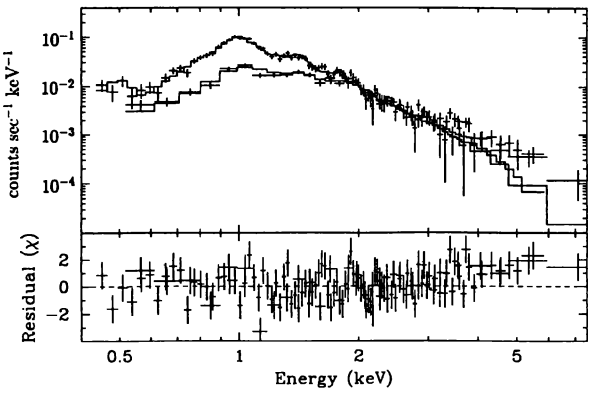

Fig. 7. GIS and SIS spectra of HCG 51 for $r < 5'$, presented in the same way as figure 4.

agrees with the value 1.15 keV predicted from the galaxy velocity dispersion of 467 km s^{-1}. The result of the Meka model gives a considerably lower iron abundance than do the other models, as has been the case with the NGC 5044 group. Moreover, it gives a temperature significantly lower than the ionization temperature determined by the Si line intensity ratios, as described later. Hence, the iron abundance of $\sim$ 0.3 solar, which was obtained by all of the models, except for the Meka model, seems to be the most likely value. This abundance is similar to those of rich clusters of galaxies. Like in the NGC 5044 group, the Si and S abundances of HCG 51 are about the same as that of Fe. The column density is inferred to be $\sim 1.6 \times 10^{21}$ cm^{-2} for all of the models, which is significantly higher than the galactic value of 1.7×10^{20} cm^{-2} (Stark et al. 1992). There seem some residuals above 3 keV, whose origin is presently unknown.

4.3. Silicon and Sulfur K lines

In the SIS spectra of the NGC 5044 group (figure 4), both He-like and H-like lines of Si and S can be clearly seen. Since the physics of the K-shell is simple, we can utilize the ratios and intensities of these lines to constrain the plasma parameters, independently of the uncertainty of the plasma emission models. We used the spectra for $4' < r < 10'$, where the spectral changes are small. By fitting the SIS spectrum with the plasma models in narrow energy ranges of 1.65–2.2 keV and 2.2–3.0 keV, we have determined the ionization temperature of the Si-K and S-K lines, respectively. The temperatures obtained with 4 models are within a quite narrow range, 1.02±0.02 keV for Si, and 1.20±0.02 keV for S. The 90% confidence range, covering all the models, is 0.91–1.14 keV for Si and 0.91–1.36 keV for S. These temperatures are consistent with those derived previously (figure 5a) by wide-band fitting using the R-S and Masai84 models, which mainly reflect the Fe-L line temperature. The best-fit Si and S abundances thus derived locally with the four plasma models exhibit a rather small scatter, 0.20–0.28 solar and 0.33–0.39 solar, respectively. Including statistical errors, the 90% confidence ranges of the Si and S abundances covering all of the four plasma models are 0.14–0.36 solar and 0.21–0.55 solar, respectively. These are generally consistent with figures 5d and 5e.

For HCG 51, only the Si lines can be used safely. The best-fit temperatures and Si abundances thus determined are quite consistent among the four plasma models, at 1.3±0.1 keV and 0.35±0.02 solar, respectively. Including statistical errors, the 90% confidence ranges of the temperature covering all the four plasma models are 1.0–1.7 keV, and that for the Si abundance is 0.15–0.60 solar. These are generally consistent with those derived previously (table 4) by wide-band fitting using the R-S, Masai84, and Masai94 model.

5. Discussion

5.1. The Mass of Hot Gas and Total Matter

Both the NGC 5044 group and HCG 51 show bright extended X-ray emission, indicating that they contain a significant amount of hot gas. The X-ray emission is extended beyond the galaxy scale, at least up to 350 kpc

Table 5. Mass and luminosity within the assumed cutoff radius $R_{\rm cut}$.*

	$R_{\rm cut}$ (kpc)	$F_{\rm X}$† (erg s^{-1} cm^{-2})	$L_{\rm X}$*† (erg s^{-1})	$M_{\rm gas}$ ($M_\odot$)	$M_{\rm galaxy}$ ($M_\odot$)	$M_{\rm total}$ ($M_\odot$)
NGC 5044 group	348 (=20′)	2.8×10^{-11}	8.6×10^{42}	1.5×10^{12}	1.6×10^{12}	1.5×10^{13}
HCG 51	367 (=7′)	1.5×10^{-12}	4.2×10^{42}	1.4×10^{12}	1.5×10^{12}	2.0×10^{13}

* $H_0 = 50$ km s^{-1} Mpc^{-1} is assumed.
† The X-ray flux $F_{\rm X}$ and luminosity $L_{\rm X}$ are both for the 0.5–10 keV band.

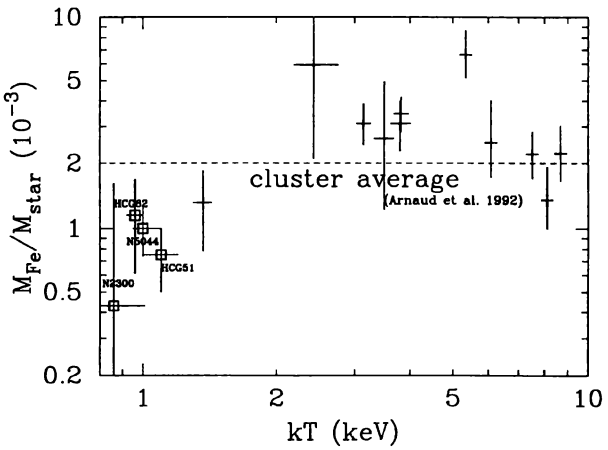

Fig. 8. $M_{\rm Fe}/M_{\rm galaxy}$ vs. gas temperature of clusters of galaxies and groups of galaxies. The crosses represent clusters of galaxies (from Tsuru 1992), while the squares represent groups of galaxies. The abundances of the NGC 2300 group and HGC 62 are $0.06^{+0.12}_{-0.05}$ solar and 0.15±0.07 solar (Mulchaey et al. 1993; Ponman et al. 1993), respectively. The galaxy mass $M_{\rm galaxy}$ of the group is $6.0\times10^{11}\,M_\odot$ for the NGC 2300 group and $7.0\times10^{11}\,M_\odot$ for HCG 62, which are estimated by assumimg a mass-to-blue-luminosity ratio of M/L_B=8.

from the group center. Since the temperature is almost constant, excluding the central region of the NGC 5044 group, isothermality may be applied for both groups. We derived the gas mass, total mass, and X-ray luminosity within about 350 kpc using the best-fit β-model parameters, and the gas temperature of 1.0 keV for the NGC 5044 group, and 1.1 keV for HCG 51. The mass of galaxies in the NGC 5044 group was taken from the integrated stellar mass-curve by David et al. (1994), which is normalized using the total optical luminosity within 500 kpc, $L_B = 2.3\times10^{11}\,L_\odot$, assuming the mass-to-light ratio of 8 $M_\odot/L_\odot$. The mass of galaxies in HCG 51 was estimated using the total optical luminosity of all 7 galaxies, $L_B = 1.9\times10^{11}\,L_\odot$ (Hickson 1993), assuming the same mass-to-light ratio. The results are summarized in table 5. The 0.5–10 keV luminosities of both objects are consistent with the ROSAT results (Ebeling et al. 1994; David et al. 1994). Although HCG 51 is about half as luminous as the NGC 5044 group, the derived X-ray luminosities are higher for both targets by an order of magnitude than those of the X-ray brightest elliptical galaxies (Forman et al. 1985). Thus, a large amount of hot gas is thought to be associated with the groups rather than individual galaxies. From these results, as well as the agreement between the X-ray temperature and the galaxy velocity dispersion, we conclude that both groups are physically bound systems.

The two groups we observed are inferred to have very similar mass components within $\sim$ 350 kpc; $M_{\rm total} \sim 2.0\times10^{13}\,M_\odot$ and $M_{\rm gas} \sim M_{\rm galaxy} \sim 1.5\times10^{12}\,M_\odot$. From ROSAT observations in comparison, the NGC 2300 group (Mulchaey et al. 1993) and HCG 62 (Ponman et al. 1993) have been shown to have $M_{\rm total} \sim 2.0\times10^{13}\,M_\odot$, $M_{\rm gas} \sim 2.0\times10^{12}\,M_\odot$, and $M_{\rm galaxy} \sim 0.8\times10^{12}\,M_\odot$ within $\sim$ 350 kpc. Thus, $M_{\rm total}$ is very similar among these 4 groups, and $M_{\rm total}$ estimated from other groups detected by ROSAT is also similar at $\sim 2.0\times10^{13}\,M_\odot$ (Mulchaey et al. 1996). This common value is larger than that of elliptical galaxies and smaller than that of clusters of galaxies. Therefore, in terms of the total gravitating matter, groups of galaxies are truly an intermediate class of systems between clusters and galaxies.

The luminous-to-total-mass ratio, $M_{\rm lum}/M_{\rm total}$, is also similar at $\sim$ 0.2 for both objects. This ratio is almost the same as those of other groups of galaxies (Mulchaey et al. 1996), clusters of galaxies, and elliptical galaxies over the total mass range of $10^{12-15}\,M_\odot$. This suggests that this value is relatively common for all hierarchical systems. However, the division of $M_{\rm lum}$ into galaxies and gas is rather scattered. For example, the ratios $M_{\rm gas}/M_{\rm galaxy}$ of the NGC 5044 group and HCG 51 are $\sim$ 1.0, while those of HCG 62 and the NGC 2300 group are 2–3. Moreover this ratio scatters in the range from 0.02–3 (Pildis et al. 1995; Mulchaey et al. 1996) among groups detected by ROSAT. Therefore, the $M_{\rm gas}/M_{\rm galaxy}$

ratio seems to scatter to a large extent among groups, even though they have very similar values of $M_{\rm total}$. This property is to be compared with the case of clusters, in which the $M_{\rm gas}/M_{\rm galaxy}$ ratio is different by a factor of only ~ 5, even though the total mass scatters by a factor ~ 100. This interesting characteristic of groups indicates that they are an intermediate class between galaxies and clusters in terms of the amount of hot gas. Considering that a large fraction of the hot gas is thought to be primordial, this feature suggests that groups are located at the threshold to confine the primordial gas. Some groups may efficiently confine the primordial gas just as clusters, while other groups may be open systems like individual galaxies. However, the $M_{\rm gas}/M_{\rm galaxy}$ ratio may also be affected by the history of the individual system evolution. In particular, it seems as if the efficiency of the galaxy formation out of the gas varies by a factors of $\sim$5 from groups to groups.

5.2. *Metal Abundances of Groups of Galaxies*

Two of the previously observed groups of galaxies, the NGC 2300 group and HCG 62, were confirmed by ASCA to have metal abundances as low as <0.2 solar (Sakima et al. 1994). However, our two objects, along with the Fornax group (Ikebe et al. 1996), have metal abundances of 0.3–0.5 solar, which are as high as those of clusters of galaxies. Therefore, the metallicity of groups seems to scatter, while clusters of galaxies have almost the same metal abundance of 0.3–0.5 solar.

Can the low metallicities of the NGC 2300 group and HCG 62 be explained as being a result of dilution by a large amount of primordial gas? In order to examine this possibility, we must investigate the ratio $M_{\rm Fe}/M_{\rm galaxy}$, where $M_{\rm Fe}$ is the iron mass in the X-ray emitting gas. This ratio means the iron production efficiency per unit galaxy mass, and/or the efficiency of metal confinement. For clusters of galaxies $M_{\rm Fe}/M_{\rm galaxy}$ is constant at $\sim 2\times10^{-3}$ (Arnaud et al. 1992; Tsuru 1992), while this ratio for elliptical galaxies is $< 1\times10^{-4}$ (Tsuru 1992). When we plot our objects on the plane of $M_{\rm Fe}/M_{\rm galaxy}$ vs. gas temperature in figure 8, together with clusters of galaxies, HCG 62, the NGC 5044 group, and HCG 51 seem to have comparable or slightly less $M_{\rm Fe}/M_{\rm galaxy}$ than clusters of galaxies. The NGC 2300 group has apparently a still lower $M_{\rm Fe}/M_{\rm galaxy}$ ratio. Therefore the low metallicity of the NGC 2300 group seems to suggest a lower efficiency of iron production and/or confinement, However, figure 8 may allow an alternative interpretation. While the abundances of the objects observed by Ginga are primarily determined by the Fe-K line, those of four groups of galaxies heavily depend on the Fe-L lines. Accordingly, any systematic difference between these two subsets could be due to the uncertainties associated with Fe-L modeling.

Under the assumption that the iron-production efficiency is the same for any system primarily comprising elliptical galaxies (Arnaud et al. 1992; Tsuru 1992), the constancy of $M_{\rm Fe}/M_{\rm galaxy}$ in clusters suggests that metal-rich gas ejected from member galaxies in clusters is almost completely bound. According to this assumption, the smaller values of $M_{\rm Fe}/M_{\rm galaxy}$ in groups, if not due to Fe-L artifact, suggest that the threshold to bind metal-rich gas ejected from member galaxies, as well as the primodial gas, lies around the class of groups of galaxies; the NGC 5044 group and HCG 51 are relatively closed systems for both primodial and metal-rich gas, while the NGC 2300 group is an open system for metal-rich gas and closed for primodial gas.

With respect to the efficiency of iron confinement, we notice in figure 8 a clear trend of decreasing $M_{\rm Fe}/M_{\rm galaxy}$ ratio as the X-ray temperature decreases (again supposing that the Fe-L discrepancy is not too severe). The temperature of the NGC 5044 group and HCG 51 is 1.0–1.3 keV, which is equivalent to their velocity dispersion of $\sigma_v \sim$450 km s^{-1}. The NGC 2300 group and HCG 62 have a temperature of 0.8–1.0 keV, which is also equivalent to their σ_v of $\sim$300 km s^{-1}. Therefore, as expected, the depth of gravitational potential seems to be a key parameter which controls the $M_{\rm Fe}/M_{\rm galaxy}$ ratio in groups.

The metal abundances of the two groups which we observed are 0.2–0.5 solar and 0.3-0.5 solar for Si and Fe respectively. Their abundance ratios may be somewhat different from those of clusters if the iron abundance determined by the Fe-L lines is correct. For clusters of galaxies, Mushotzky (1994) and Mushotzky et al. (1996) have shown that the Si-to-Fe abundance ratio is about two-times larger than that of our two objects. Probably the difference in the abundance ratio between clusters and groups reflects some differences in their dynamical and chemical evolution, e.g., the relative importance of Type-I and Type-II supernovae.

We note that both of our groups clearly exhibit the β discrepancy (Bird et al. 1995). That is, the ratio of the temperature to the velocity dispersion, $\beta_{\rm spec}$, is ~ 1, while the slope of the surface brightness law, $\beta_{\rm fit}$, is considerably flatter. This may be consistent with models in which the relative amount of energy injected by non-gravitational processes is a large fraction of the binding energy.

5.3. *Comparison between the NGC 5044 Group and HCG 51*

In the optical image, the NGC 5044 group and HCG 51 show quite different features, e.g., in the total number of member galaxies. Nevertheless, the gas mass and total mass are very similar between them. Therefore, the amount of hot gas does not seem to depend on the number of member galaxies. However, the dominant galaxies

in both groups are elliptical galaxies; this may be responsible for the large X-ray luminosities of these systems, as suggested by Mulchaey et al. (1996). The NGC 2300 group and HCG 62 also have dominant elliptical galaxies.

On the other hand, whether it has a cD galaxy or not is another important difference between the NGC 5044 group and HCG 51, which seems to lead to some differences in the X-ray properties. The NGC 5044 group has a sharper X-ray profile and a higher central X-ray brightness than does HCG 51, and shows a temperature decrease in the center. Furthermore, there is some hint of a Fe abundance increase in the central region of the NGC 5044 group (figure 5f). Very similar properties were observed from the Centaurus cluster (Fukazawa et al. 1994) and the Virgo cluster (Koyama et al. 1991; Matsumoto et al. 1996), which also have cD galaxies. These properties of the NGC 5044 group and their absence in HCG 51 may be attributed to the presence of the central dominant galaxy, NGC 5044, and the absence of such a dominant member in HCG 51, respectively.

From both targets, we detected significant excess absorption on the order of $\sim 1 \times 10^{21}$ cm^{-2} , whose precise value is somewhat sensitive to the choice of the plasma model. The excess absorption in the NGC 5044 group is concentrated at the group center, and may be associated with the cooling flow. However, that seen in HCG 51 might be of somewhat different origin, since the radiative cooling time of the gas at the center of HCG 51 is estimated to be 8 Gyr: this is comparable to the Hubble time, and at least by an order of magnitude longer than that at the center of the NGC 5044 group.

6. Conclusion

We observed two groups of galaxies, the NGC 5044 group and HCG 51, with ASCA. Extended soft X-ray emission from hot gas was detected from both of them. The temperature of the hot gas is ~1 keV for both objects, which is equivalent to their optical velocity dispersion. The X-ray luminosity in the 0.5–10 keV band is 1×10^{43} erg s^{-1} for the NGC 5044 group and 5×10^{42} erg s^{-1} for HCG 51, which are higher by an order of magnitude than those of X-ray bright elliptical galaxies. These X-ray features indicate that the hot gas is associated with the large-scale gravitational potential of these groups of galaxies.

Both objects have $M_{\rm total} \sim 2.0 \times 10^{13} M_\odot$ and $M_{\rm gas} \sim M_{\rm galaxy} \sim 1.5 \times 10^{12} M_\odot$. The ratios among these mass components are $M_{\rm gas}/M_{\rm galaxy} \sim 1$ and $M_{\rm lum}/M_{\rm total} \sim 0.2$ within ~ 350 kpc. The latter is similar to the many groups observed by ROSAT; this value is further thought to be rather common for various hierarchical classes of systems. The former scatters considerably among groups, indicating that the efficiency of binding primordial gas or the condition of galaxy formation is different among groups of galaxies. $M_{\rm total}$ is larger than that of elliptical galaxies and smaller than that of clusters of galaxies. Therefore, in view of the total gravitating matter, groups of galaxies form an intermediate class of systems between clusters and galaxies.

For both objects, the metal abundance is 0.3–0.5 solar, which is a typical value for clusters of galaxies and significantly higher than those of the NGC 2300 group and HCG 62. Therefore, the metal abundance also scatters amongst groups of galaxies. The ratio $M_{\rm Fe}/M_{\rm galaxy}$ of groups of galaxies seems to positively correlate with the temperature, in other words, the depth of the gravitational potential, if the iron abundance determined by Fe-L lines is correct. The Si abundance is about the same as the Fe abundance, in contrast to some clusters in which the Si abundance appears to be higher than the Fe abundance (in reference to the solar photospheric value).

Although the two groups studied exhibit fairly similar X-ray properties in spite of the different numbers of galaxies, the NGC 5044 group has a sharper X-ray surface brightness than HCG 51 and exhibits a temperature decrease in the center together with a hint of an iron abundance gradient. These features may be associated with the cD galaxy NGC 5044.

The authors are grateful to Dr. K. Masai for helpful discussions about plasma emission models, to Dr. N. Arimoto for useful comments, and to the ASCA team for their efforts on the operation and calibration.

References

Anders E., Grevesse N. 1989, Geochim. Cosmochim. Acta 53, 197
Arimoto N. 1996, Proc. IAU Symp. No.171
Arnaud M., Raymond J. 1992, ApJ 398, 394
Arnaud M., Rothenflug R. 1985, A&AS 60, 425
Arnaud M., Rothenflug R., Boulade O., Vigroux L., Vangioni-Flam E. 1992, A&A 254, 49
Awaki H., Koyama K., Kunieda H., Takano S., Tawara Y., Ohashi T. 1991, ApJ 366, 88
Awaki H., Mushotzky R.F., Tsuru T., Fabian A.C., Fukazawa Y., Loewenstein M., Makishima K., Matsumoto H. et al. 1994, PASJ 46, L65
Bird C., Mushotzky R.F., Metzler C. 1995, ApJ 453, 40
Burke B.E., Mountain R.W., Harrison D.C., Bautz M.W., Doty J.P., Ricker G.R., Daniels P.J. 1991, IEEE Trans. ED-38, 1069
Cavaliere A., Fusco-Femiano R. 1976, A&A 49, 137
David L.P., Jones C., Forman W. 1995, ApJ 445, 578
David L.P., Jones C., Forman W., Daines S. 1994, ApJ 428, 544
Ebeling H., Voges W., Böhringer H. 1994, ApJ 436, 44
Edge A.C., Stewart G.C. 1991, MNRAS 252, 414
Fabbiano G., Kim D.-W., Trinchieri G. 1992, ApJS 80, 531

Fabian A.C., Arnaud K.A., Bautz M.W., Tawara Y. 1994, ApJL 436, L63
Ferguson H.C., Sandage A. 1990, AJ 100, 1
Forman W., Jones C., Tucker W. 1985, ApJ 293, 102
Fukazawa Y., Ohashi T., Fabian A.C., Canizares C.R., Ikebe Y., Makishima K., Mushotzky R.F., Yamashita K. 1994, PASJ 46, L55
Hatsukade I. 1989, Ph.D. Thesis, Osaka University
Henriksen M.J., Mamon G.A. 1994, ApJ 421, L63
Hickson P. 1993, Astrophys. Lett. Commun. 29, 1
Hickson P., Kindl E., Huchra J.P. 1988, ApJ 331, 64
Ikebe Y., Ezawa H., Fukazawa Y., Hirayama M., Ishisaki Y., Kikuchi K., Kubo H., Makishima K. et al. 1996, Nature 379, 427
Jones C., Forman W. 1984, ApJ 276, 38
Kato K., Masai K. 1984, Ap&SS 98, 267
Kohmura Y., Fukazawa Y., Ikebe Y., Ishisaki Y., Kamijo S., Kaneda H., Makishima K., Matsushita K. et al. 1993, Proc SPIE 2006, 79
Koyama K., Takano S., Tawara Y. 1991, Nature 350, 135
Masai K. 1984, Ap&SS 98, 367
Matsumoto H., Koyama K., Awaki H., Tomita H., Tsuru T., Mushotzky R.F., Hatsukade I. 1996, PASJ 48, 201
Matsushita K., Makishima K., Awaki H., Canizares C.R., Fabian A.C., Fukazawa Y. et al. 1994, ApJL 436, L41
Mewe R., Gronenschild E.H.B.M., van den Oord G.H.J. 1985, A&AS 62, 197
Mewe R., Lemen J.R., van den Oord G.H.J. 1986, A&AS 65, 511
Mulchaey J.S., Davis D.S., Mushotzky R.F. 1993, ApJL 404, L9
Mulchaey J.S., Davis S.S., Mushotzky R.F., Burstein D. 1996, ApJ 456, 80
Mushotzky R.F. 1994, in New Horizon in X-ray Astronomy, ed F. Makino, T. Ohashi (Universal Academy Press, Tokyo) p243
Mushotzky R.F., Loewenstein M., Arnaud K.A., Tamura T., Fukazawa Y., Matsushita K., Kikuchi K., Hatsukade I. 1996, ApJ in press
Ohashi T., Ebisawa K., Fukazawa Y., Hiyoshi K., Horii M., Ikebe Y., Ikeda H., Inoue H. et al. 1996, PASJ 48, 157
Ohashi T., Makishima K., Ishida M., Tsuru T., Tashiro M., Mihara T., Kohmura Y. 1991, Proc SPIE 1549, 9
Pildis R.A., Bregman J.N., Evrard A.E. 1995, ApJ 443, 514
Ponman T.J., Bertram D. 1993, Nature 363, 51
Raymond J.C., Smith B.W. 1977, ApJS 35, 419
Rothenflug R., Arnaud M. 1985, A&A 147, 337
Sakima Y., Tawara Y., Yamashita K. 1994, in New Horizon in X-ray Astronomy, ed F. Makino, T. Ohashi (Universal Academy Press, Tokyo) p557
Stark A.A., Gammie C.F., Wilson R.W., Bally J., Linke R.A. 1992, ApJS 79, 77
Tanaka Y., Inoue H., Holt S.S. 1994, PASJ 46, 37
Tsuru T. 1992, Ph.D. Thesis, University of Tokyo
Tsusaka Y., Sakima Y., Yamashita K. 1994, in New Horizon in X-ray Astronomy, ed F. Makino, T. Ohashi (Universal Academy Press, Tokyo) p563
White D.A., Fabian A.C., Johnstone R.M., Mushotzky R.F., Arnaud K.A. 1991, MNRAS 252, 72